Phase Transition and Transition Kinetics of a Thermotropic Poly(amide−imide) Derived from 70% Pyromellitic Dianhydride, 30% Terephthaloyl Chloride, and 1,3-Bis[4-(4′-aminophenoxy)cumyl]benzene

S. L. Liu,[†,‡] T. S. Chung,*[,†,‡] J. X. Geng,[§] E. L. Zhou,[§] and S. Tamai[⊥]

Institute of Materials Research and Engineering, 3 Research Link, Singapore 117602; Department of Chemical & Environmental Engineering, National University of Singapore, 10 Kent Ridge Crescent, Singapore 119260; Changchun Institute of Applied Chemistry, Chinese Academy of Sciences, Changchun 130022, China; and Material Science Laboratory, Mitsui Chemicals, Inc., 580-32 Nagaura Sodegaura-City, Chiba 299-0265, Japan

Received May 22, 2001; Revised Manuscript Received August 24, 2001

ABSTRACT: The phase transition and transition kinetics of a liquid crystalline copoly(amide−imide) (PAI37), which was synthesized from 70 mol % pyromellitic dianhydride, 30 mol % terephthaloyl chloride, and 1,3-bis[4-(4′-aminophenoxy)cumyl]benzene, was characterized by differential scanning calorimetry, polarized light microscopy, X-ray diffraction, and rheology. PAI37 exhibits a glass transition temperature at 182 °C followed by multiple phase transitions. The crystalline phase starts to melt at ∼220 °C and forms smectic C (S_C) phase. The S_C phase transforms into smectic A (S_A) phase when the temperature is above 237 °C. The S_C to S_A transition spans a broad temperature range in which the S_A phase vanishes and forms isotropic melt. The WAXD fiber pattern of PAI37 pulled from the anisotropic melt revealed an anomalous chain orientation, which was characterized by its layer normal perpendicular to the fiber direction. The transition kinetics for the mesophase and crystalline phase formation was also studied.

1. Introduction

Liquid crystalline polyimide is a relatively new area of study in polymer science,[1] although aromatic amorphous and crystalline polyimides have found a variety of applications,[2] such as thermoplastic films, thermosetting resins, and insulating and dielectric materials. Among various dianhydrides used for polyimide synthesis,[3] pyromellitic dianhydride (PMDA) shows a flat, linear, and rigid structure and therefore is expected to be a good mesogen for mesophase formation. However, early systematic studies on polyimides derived from PMDA and aliphatic diamines indicated that PMDA was not a mesogenic unit.[4] Other symmetric imide groups were also proved to be almost nonmesogenic.[5] On the contrary, the asymmetric ester−imide group, *N*-[4-(chloroformyl)phenyl]-4-(chloroformyl) phthalimide, has demonstrated to be a good mesogenic unit which could form mesophases through reactions with a variety of diols,[6−10] although the homopolymer, poly[4-(hydroxyphenyl)trimellitic acid imide], did not exhibit liquid crystallinity due to its high melting temperature.[11] Interestingly, quite a number of liquid crystalline poly(ester−imide)s derived from this ester−imide group exhibit layered smectic structures.[12−15] In a later attempt to synthesize liquid crystalline polyimide from PMDA, it was found that the combination of PMDA with a ester-free diamine, 1,3-bis[4-(4′-aminophenoxy)cumyl]benzene (BACB), which is also nonmesogenic, could form a stable smectic phase upon melting.[16−20] However, like other PMDA-based aromatic polyimides, this liquid crystalline polyimide, PMDA−BACB, shows very poor solubility in common organic solvents. On the other hand, the reaction of BACB with terephthaloyl chloride (TPC) can produce a polyamide, which is soluble in *N*-methyl-2-pyrrolidone (NMP) at room temperature. The combination of liquid crystallinity from PMDA−BACB and good solubility from TPC−BACB would offer the random copolyamideimide advantages over the homopolymers. In fact, the copoly(amide−imide) derived from 70 mol % PMDA, 30 mol % TPC, and BACB exhibits both thermotropic property and solubility in warm NMP, which will be presented in this work.

Study on phase transitions in main chain liquid crystalline polymers is a very interesting subject, and enormous efforts on understanding these transitions have been made.[21−33] As the majority of liquid crystalline polymers are polyesters or copolyesters based on 4-hydroxybenzoic acid (HBA), systematic investigation on the phase behavior of liquid crystalline polyimides is still lacking due to the very rare availability of liquid crystalline polyimide samples. Pardey et al.[26−28] studied the liquid crystal transition, ordered structure, and crystallization kinetics in a series of thermotropic poly(ester imide)s synthesized from *N*-[4-(chloroformyl)phenyl]-4-(chloroformyl) phthalimide and the respective diols with the number of methylene groups (*n*) varying from 4 to 12. Kim et al.[29−31] synthesized and characterized a series of liquid crystalline poly(ester−imide)s derived from *N*-(*ω*-carboxyalkylene) trimellitic imides. However, most of these poly(ester−imide)s are monotropic, and their mesophase could only be achieved during cooling. Leland et al.[32,33] investigated the phase transition behavior and anomalous chain orientation in the copoly(ester−imide)s derived from *N*,*N*′-dodecane-1,12-diylbis(trimellitimide) and two acetylated diols, hydroquinone and 4,4′-dihydroxybiphenyl. Studies by Schwarz[34] and Tanaka[35] on the liquid crystalline polyimide PMDA−BACB have led to controversy. Schwarz et al.,[34] on the basis of their synchrotron radiation results, indicated that the mesophase was a S_A phase,

† Institute of Materials Research and Engineering.
‡ National University of Singapore.
§ Chinese Academy of Sciences.
⊥ Mitsui Chemicals, Inc.
* Corresponding author: E-mail chencts@nus.edu.sg; Fax 65-7797936.

10.1021/ma010895f CCC: $20.00
Published on Web 11/01/2001

Chart 1. Chemical Structures of Monomers and Liquid Crystalline Copoly(amide−imide) (PAI37)

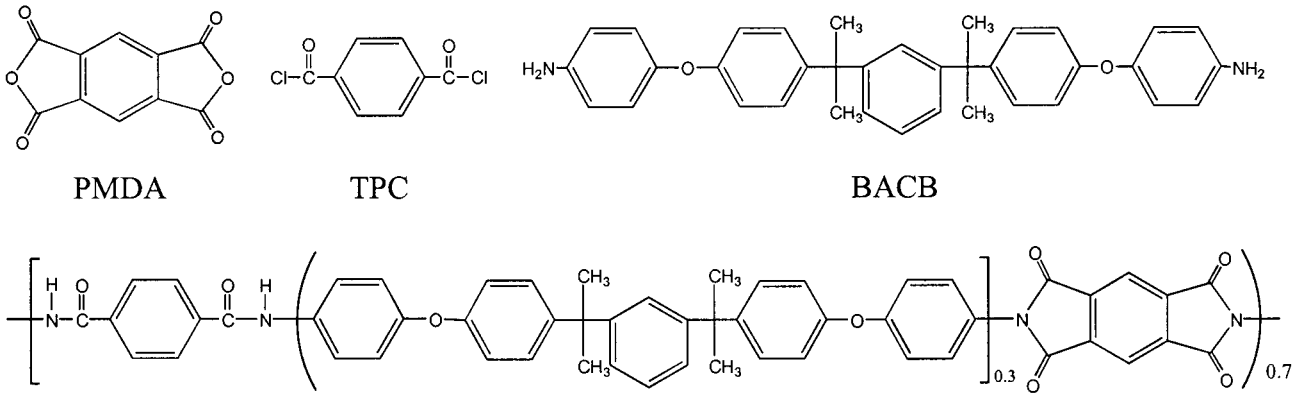

and possibly the solid sample contained a more ordered S_B phase. However, Tanaka et al.[35] pointed out that the filament extruded from the anisotropic phase had a structure similar to S_C phase and that extruded and melt-drawn from the isotropic phase had a structure similar to S_A phase.

In a series of studies on the crystallization and phase transition behavior of a liquid crystalline polyimide derived from BACB, we have investigated the novel crystallization morphology, crystallization kinetics, and double melting behavior of the homopolyimide (PMDA−BACB).[36−38] In this paper, we will report the phase transition and transition kinetics of a copoly(amide−imide) containing 70 mol % PMDA and 30 mol % TPC.

2. Experiments

2.1. Materials. The thermotropic liquid crystalline copoly(amide−imide) (denoted as PAI37), which was synthesized from 1,2,4,5-benzentetracarboxylic dianhydride (PMDA) (70 mol %), terephthaloyl chloride (TPC) (30 mol %), and 1,3-bis-[4-(4′-aminophenoxy)cumyl]benzene (BACB), was kindly provided by Mitsui Chemicals Co. The detailed synthesis procedures of PAI37 were reported elsewhere.[17−20] The inherent viscosity of this copolymer was measured to be 1.15 dL/g in a 9:1 mixed solvent of 4-chlorophenol and phenol at 0.5 g/100 mL at 308 K. The chemical structures of the monomers and PAI37 are shown in Chart 1. The polymer was dried at 120 °C in a vacuum oven for 24 h before use.

2.2. Differential Scanning Calorimetry (DSC). Thermal measurements were carried out using a Perkin-Elmer Pyris-1 DSC. For nonisothermal crystallization study, the samples were heated or cooled between 50 and 340 °C at various rates of 5, 10, 20, 40, and 80 °C/min. For isothermal transition kinetics study, the samples were melted at 340 °C for 2 min and then cooled at 40 °C/min to the crystallization temperatures. The exothermic traces as a function of time and the subsequent heating curves as a function of temperature were recorded. All tests were run under nitrogen purge. The instrument was calibrated with high-purity indium and zinc.

2.3. Polarized Light Microscopy (PLM). The morphological development of this poly(amide−imide) PAI37 was observed with an Olympus BX50 microscope coupled with a Linkam TP93 hot stage. The powder sample was sandwiched between two glass slides on a hot plate preheated to 340 °C and then pressed and quenched to room temperature in air before morphology observation. The time evolution of liquid crystal texture was recorded at the liquid crystallization temperature. To observe the banded texture, the powder sample was sheared between two glass slides on a hot plate at different temperatures and then quenched to room temperature on a cold brass plate.

2.4. Wide-Angle X-ray Diffraction (WAXD). The temperature variable wide-angle X-ray diffraction (WAXD) experiments on the melt-quenched sample were performed on a

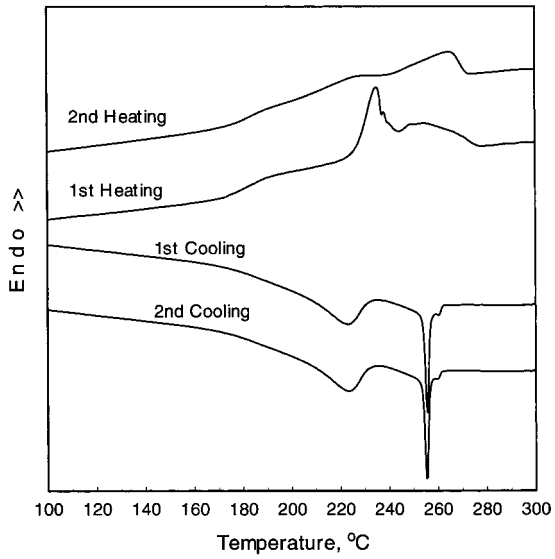

Figure 1. Typical heating and cooling curves for PAI37.

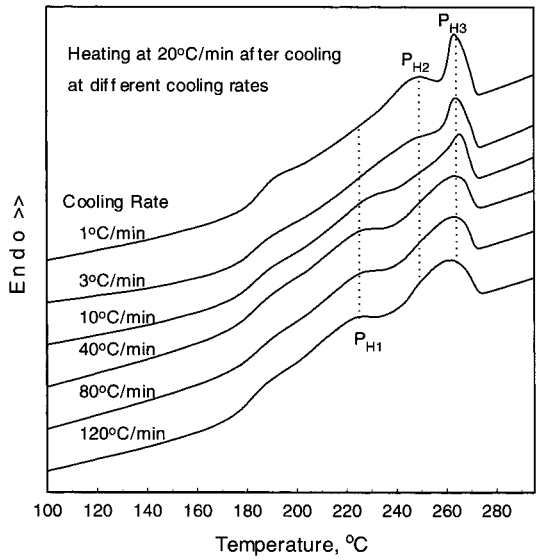

Figure 2. Heating curves for PAI37 subjected to different cooling histories.

Bruker D8 advanced diffractometer. A step of 0.02° was used in all scans from 2° to 40°. Ni-filtered Cu Kα radiation with a wavelength of $\lambda = 1.5604$ Å was used in the experiments. The powder diffraction profile was recorded using a slit recorder, and the heating rate was 10 °C/min. The fiber diffraction pattern was recorded using a Bruker general-area-detector diffraction system (GADDS) at room temperature. To focus on

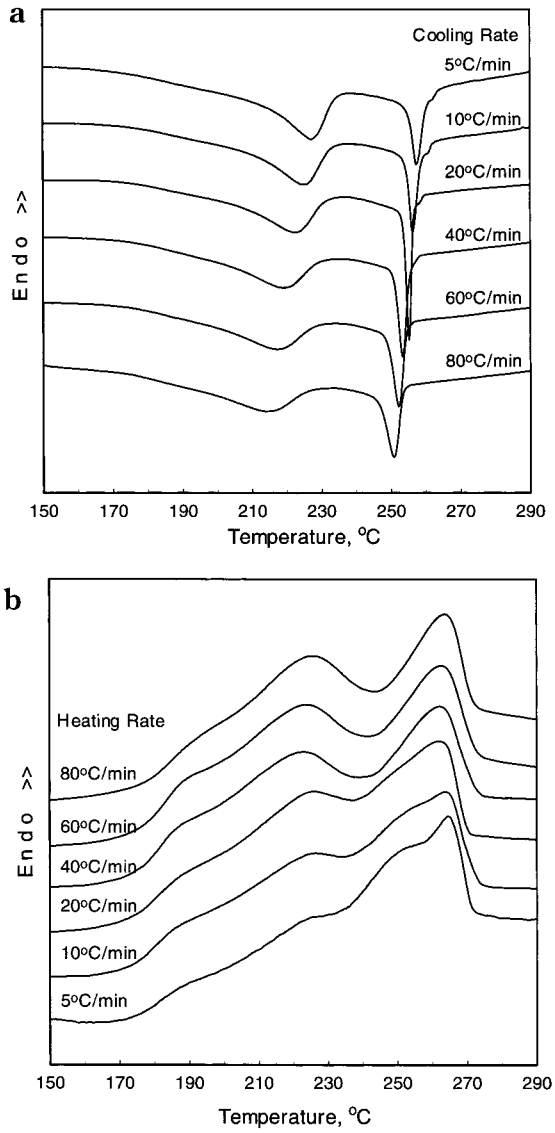

Figure 3. (a) Set of DSC cooling traces for PAI37 at different cooling rates. (b) Set of DSC heating traces for PAI37 at different heating rates (the sample was cooled from the isotropic melt using the corresponding heating rate).

the scattering from the low angle, the distance between the sample and the detector was kept 30 cm.

2.5. Rheological Characters. The rheological experiments were conducted on an AERS rheometer, and the cone and plate fixture with a diameter of 25 mm was used. To avoid the effect of sample loading on the rheological behavior, the sample was loaded at 320 °C, which is much higher than the isotropization temperature. Temperature sweep experiments were performed at a rate of 5 °C/min and an oscillatory frequency (ω) of 6.28 rad/s. Time sweep for isothermal crystallization study was conducted at a strain of 1% to ensure linear viscoelasticity and at a frequency of 6.28 rad/s. The fine powder sample was cold-pressed into a 25 mm disk by using a die to facilitate the sample loading in the rheological experiments.

2.6. Thermogravimetric Analysis (TGA). The weight loss of the copoly(amide−imide) during heating in the air environment was measured on a Perkin-Elmer thermogravimetric analysis system TGA-7 at 20 °C/min. PAI37, similar to the homopolyimide and homopolyamide,[39] exhibits very good thermal stability below 400 °C and begins to decompose around 450 °C. The 5% weight loss temperature is about 520 °C. For PLM, DSC, and rheology experiments the maximum operating temperature is 340 °C, which is much lower than the decomposition temperature.

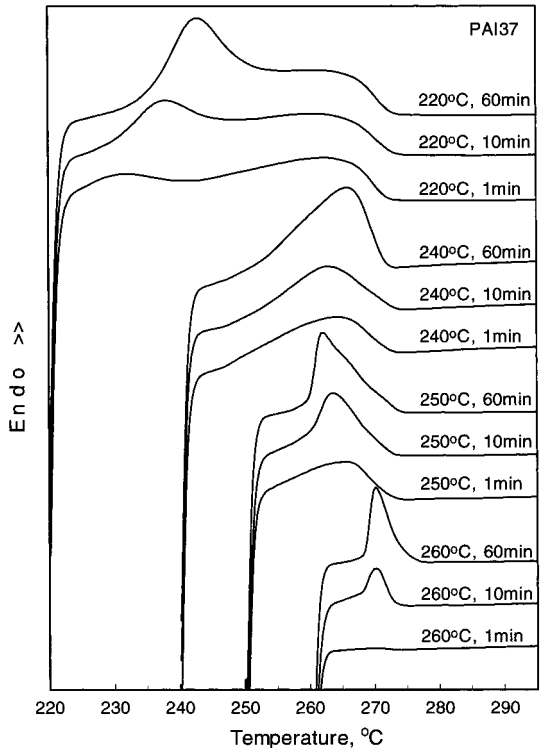

Figure 4. DSC heating curves for PAI37 kept at different temperatures for different times.

Table 1. Thermal Transitions Observed by Different Methods during Heating

method	transition 1	transition 2	transition 3
DSC[a]	P_{H1}, K → S_C	P_{H2}, S_C → S_A	P_{H3}, S_A → I
	T_{onset} = 206.8 °C	T_{onset} = 236 °C	T_{onset} = 262 °C
	T_{peak} = 225.2 °C	T_{peak} = 255 °C	T_{peak} = 265 °C
	ΔH = 1.67 J/g	ΔH = 4.42 J/g	ΔH = 0.70 J/g
PLM[b]	220−230 °C	235−260 °C	260−285 °C
rheology[b]	220−235 °C	235−263 °C	263−274 °C

[a] P_{H1}, P_{H2}, and P_{H3} are shown in Figure 2. [b] Temperature range.

3. Results and Discussion

3.1. Phase Transition Behavior. Figure 1 shows the typical DSC heating and cooling traces at a rate of 20 °C/min between 50 and 340 °C. During the first heating of the as-polymerized sample, a glass transition (T_g) appears around 182 °C and is followed by a sharp endotherm at 235 °C and a broad one at 258 °C. In the first cooling process, a small exothermic process occurs around 262 °C and is followed by a strong and sharp exothermic peak at 255 °C and a broad exothermic process from 235 to 200 °C (peak temperature 223 °C), which is just about 20 °C higher above the T_g. In the second heating, the T_g remains unchanged at 182 °C, while the first endothermic peak around 225 °C becomes very weak (ΔH = 1.67 J/g) and the second endothermic peak shifts to 264 °C (ΔH = 5.12 J/g). It is noticed from the second heating curve that the second endothermic peak is asymmetric and has a long initial endothermic process, suggesting that this peak may consist of two overlapped endothermic processes. The second cooling curve is very similar to the first cooling one. The big differences in the first and second heating curves are normally caused by the thermal history in the as-polymerized samples, which have been observed in many crystalline and liquid crystalline polymers.[8−10] In order for all DSC samples to possess the same thermal history, all the samples were first melted at 340 °C for

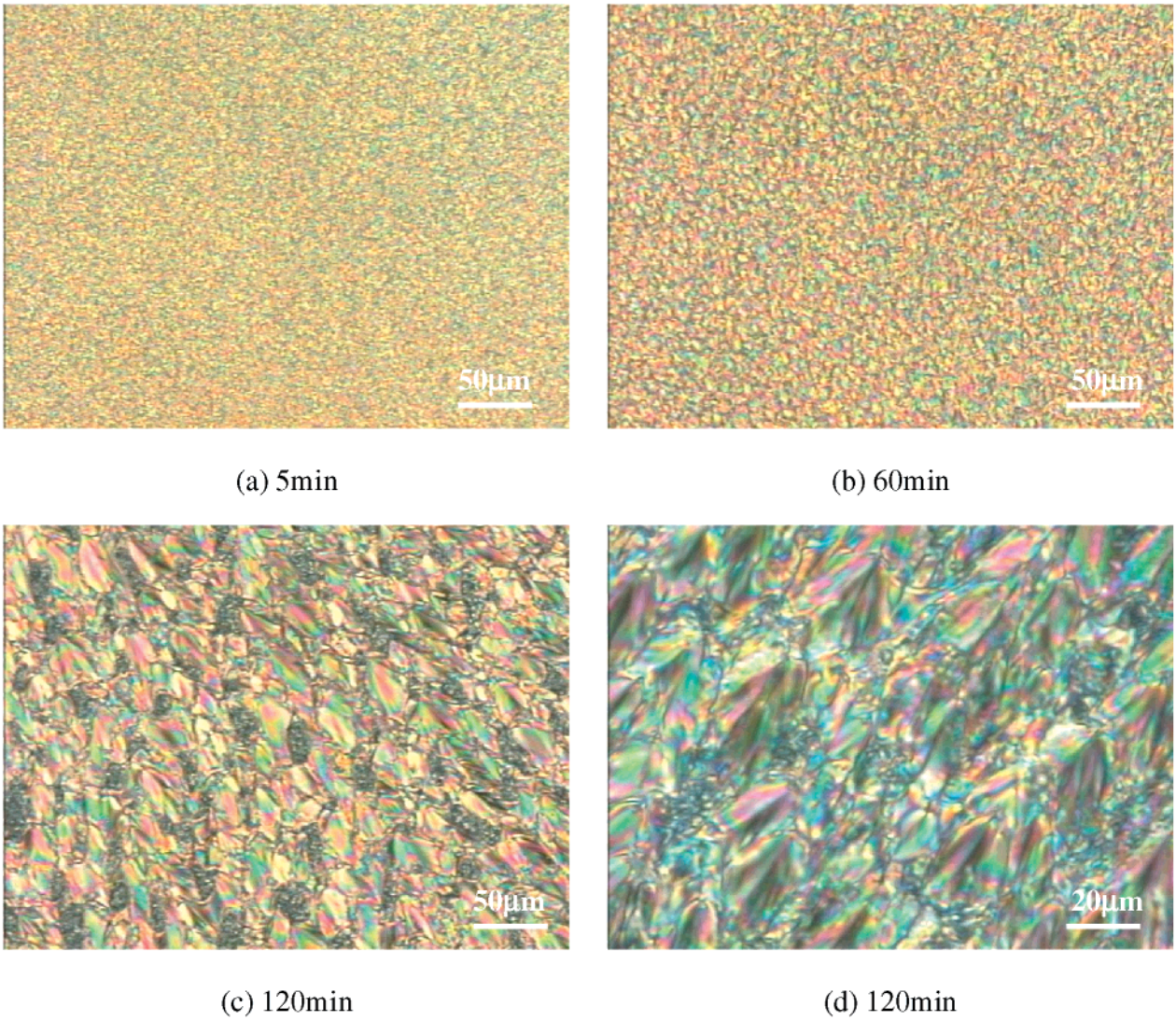

Figure 5. Evolution of liquid crystalline texture at 260 °C.

2 min and then cooled to 50 °C at 100 °C/min as the initial samples unless specified individually. Careful examination of the second cooling and heating curves in Figure 1 reveals that the first onset transition temperature in the cooling curve is about 262 °C, which is higher than the onset temperature of the broad transition (about 236 °C) in the heating curve. This is also an indication that the broad transition from 230 to 273 °C in the second heating curve is an overlapped transition and/or a biphasic phenomenon. Figure 2 shows the heating curves at a rate of 20 °C/min for the samples subjected to different cooling histories from 1 to 120 °C/min. All the three melting peaks (denoted as P_{H1}, P_{H2}, and P_{H3} from low to high temperature) show some dependency on the cooling histories. When the cooling rate is higher than 10 °C/min, P_{H1} is obvious, while P_{H2} and P_{H3} are overlapped and form a "round peak". When the cooling rate is lower than 10 °C/min, P_{H1} (∼220 °C) is almost indiscernible, while P_{H2} and P_{H3} are gradually separated and P_{H3} sharpens when the sample was cooled with a rate of 1 °C/min. After deconvolution of P_{H2} and P_{H3} in the heating process, P_{H3} has an onset transition temperature around 262 °C, which agrees very well with the highest onset transition in the cooling curve. This result supports the coexistence of two phases (P_{H2} and P_{H3}).[40]

Figure 3 shows the normalized cooling and heating traces for PAI37. The heating curve was recorded immediately after the sample was cooled using the same rate. In the cooling curves shown in Figure 3a, the small exothermic peak that appears at the highest transition temperature is observed as long as the cooling rate is not higher than 40 °C/min. The onset transition temperature (∼262 °C) of this exothermic peak agrees well with that of P_{H3}. The sharp transition at 255 °C exhibits little cooling rate dependence, which shifts about 3 °C when the cooling rate is increased from 5 to 80 °C/min. The third broad peak moves about 14 °C when the cooling rate is increased from 5 to 80 °C/min, indicating that this transition is associated with the formation of a highly ordered solid phase. When the heating rate is high, P_{H1} and P_{H3} are obvious (Figure 3b), while P_{H1}, P_{H2}, and P_{H3} all can be observed when a mediate to low heating rate is employed. Comparing parts a and b of Figure 3, it seems that the lowest endothermic peak in Figure 3b (the onset temperature is about 210 °C) has no corresponding exothermic peak observable in Figure 3a, which could be embedded in the long tail of the broad exothermic process.

Some representative heating curves for PAI37 isothermally kept for different times at several temperatures are plotted in Figure 4. These temperatures were

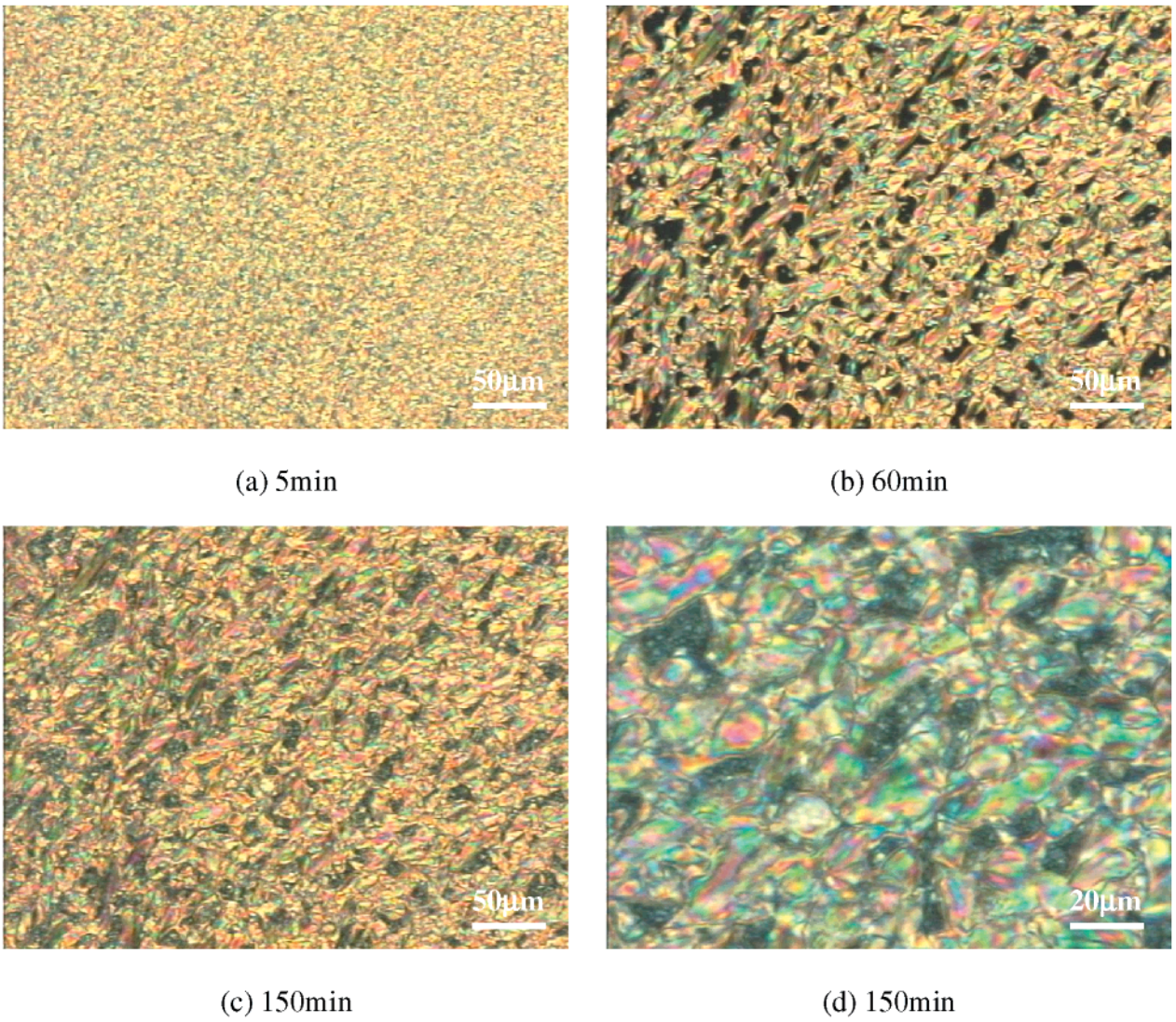

Figure 6. Evolution of liquid crystalline texture at 268 °C.

chosen on the basis of the cooling curve in Figure 1. At 260 °C, the amplitude of the endothermic peak is found to increase with time gradually. It seems that this transition is a kinetically controlled process as the amplitude increases with time. The transition behavior for PAI37 kept at 250 °C is different in that the endothermic peak for the sample held for a very short time is flat and broad. The peak temperature moves to a lower temperature first when the holding time is shorter than 60 min and then moves to a higher temperature. Isothermal holding around 240−235 °C, which lies between the two main exothermic processes in the cooling curve shown in Figure 1, is the process for the mesophase to develop more fully. The endothermic peak due to the growth of mesophase would slightly shift to a higher temperature. Further decreasing the holding temperature below 230 °C, the crystalline phase or the highly ordered solid phase (P_{H1} in Figure 2) could be gradually grown with time. The transition processes of P_{H2} and P_{H3} are not influenced by the holding time.

From these heating curves, three temperature regions can be obtained: (1) $T_c \geq 260$ °C, (2) 240 °C $\leq T_c <$ 260°C, and (3) $T_c \leq 230$ °C. When the T_c is higher than 260 °C but lower than 267 °C, the endothermic peak is symmetric and moves to high temperature with increasing T_c, but the peak area is reduced. When the T_c falls between 260 and 240 °C, the endothermic peak is asymmetric and gradually changes its shape from titling to the left to titling to the right. When the T_c is lower than 230 °C, three transitions are observed. P_{H1} is highly dependent on T_c, while the broad endothermic peak (overlapped P_{H2} and P_{H3}) at higher temperature is independent of T_c.

The above DSC characterization from Figures 1−4 demonstrates that there are three transitions. These transitions are summarized in Table 1. From the DSC results, there are three possibilities corresponding to the three transitions observed: (1) K → S_A → N → I; (2) K → S_C → S_A → I; (3) K → S_C → N → I. Here, K refers to a true crystalline phase or a highly ordered solid smectic phase, and I means isotropic melt. Which route is possible? More results from other experiments are needed to gain more insight into these phase transitions and identify the mesophases. One point, however, is certain that the lowest endotherm is a transition from a crystal or a highly ordered solid smectic phase to a mobile smectic phase.

The morphology of PAI37 changes rapidly during dynamic heating. The quenched sample exhibits birefringence at room temperature. Upon heating at 20 °C/min, the texture remains unchanged before 220 °C at which the field turns into yellowish and then dark red.

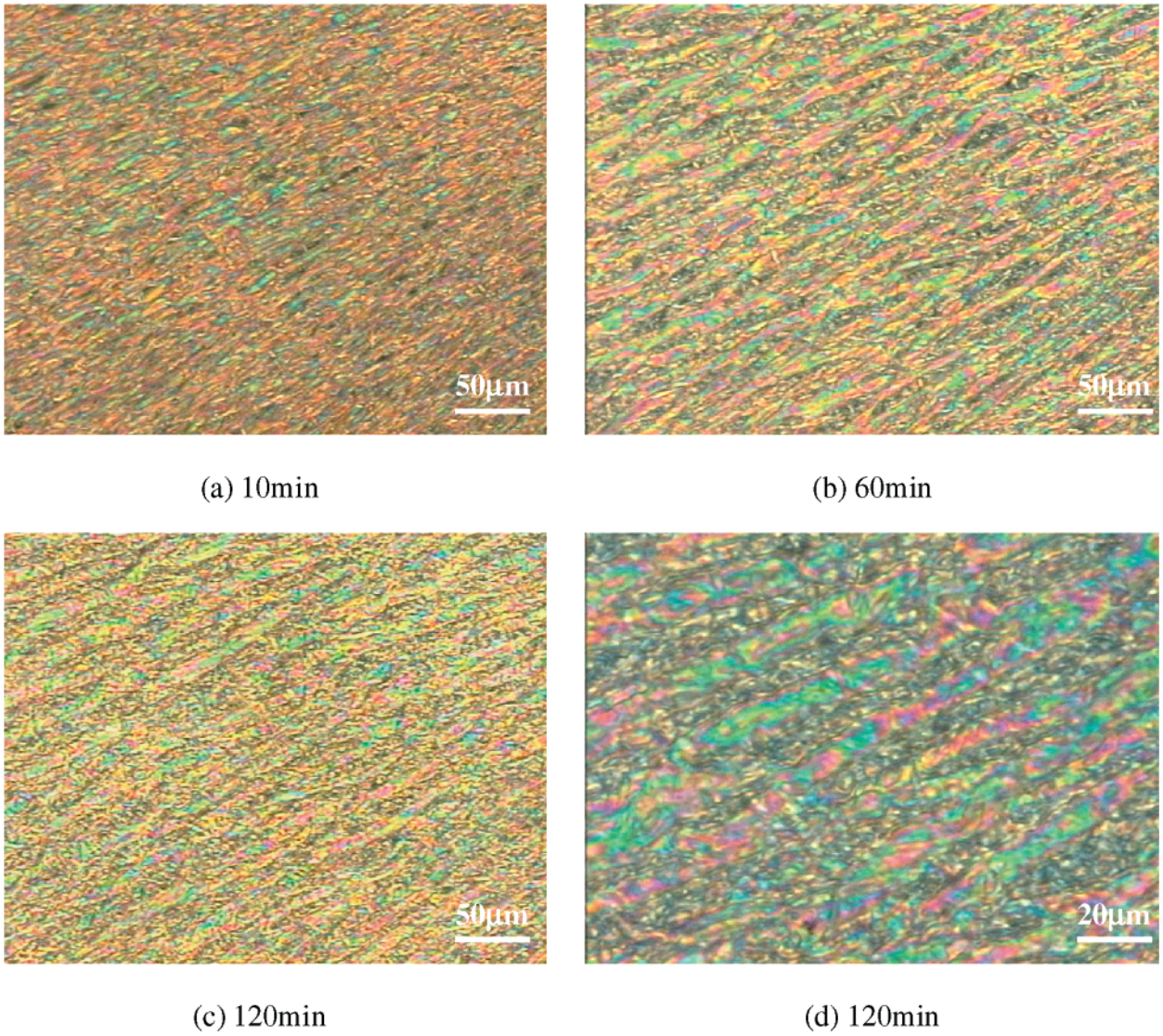

Figure 7. Liquid crystalline texture developed by annealing at 269 °C.

The color is changed again upon heating to 250 °C. Finally, the sample melts completely when it is heated above 285 °C. During the cooling process followed, the sample starts to show birefringence at 265 °C. The color of the field becomes darker when it is cooled to 260 °C, after which there is no further morphological changes observable under crossed polars. The transition temperatures shown as color changes under the polarized light microscope are generally consistent with that observed in the DSC experiments (Table 1). However, because of the high viscosity of the smectic phase and the limited resolution by the optical microscope, no convincing morphologies associating with the mesophases can be provided in the dynamic heating or cooling experiments.

Figures 5 and 6 provide two sets of pictures depicting the evolution of the liquid crystalline textures developed at 260 and 268 °C, respectively. The focal-conic fan texture developed at 260 °C unambiguously demonstrates the existence of S_C phase.[41,42] PAI37, on this point, shows similarity to the liquid crystalline homopolyimide.[35] The texture developed at 268 °C includes both isotropic and anisotropic domains as at this temperature the transition from mesophase to isotropic melt can take place. To further identify the mesophase formed at the highest temperature, the sample was heated to isotropic temperature and quickly cooled to 269 °C and then hold at this temperature. The texture developed by annealing at 269 °C as shown in Figure 7 clearly shows the homeotropic domains, indicating the existence of S_A phase. In fact, the needlelike structure, which was observed before isotropization in the dynamic heating, is also an indication of the S_A phase. Therefore, the phase transitions in PAI73 during heating could be preliminarily concluded as K → S_C → S_A → I. As the transition from S_C to S_A (or from S_A to S_C) would inevitably involve in the reorientation of the molecular chains from tilting to paralleling to the layer normal, this process is indeed a kinetic one, which has been reported in a few cases.[43] The broadness of the transition temperature from S_C to S_A in the heating process could be resulted from the higher interchain frictions due to the high viscosity as characterized in the rheological characterization section.

The wide-angle X-ray diffraction profiles during heating and cooling are displayed in Figure 8. At low temperatures, two major contributions to the scatterings are observed in the middle- and wide-angle regime. The middle-angle X-ray scattering (MAXS) found at a scattering angle of $2\theta \approx 2.92°$ corresponds to a d spacing of

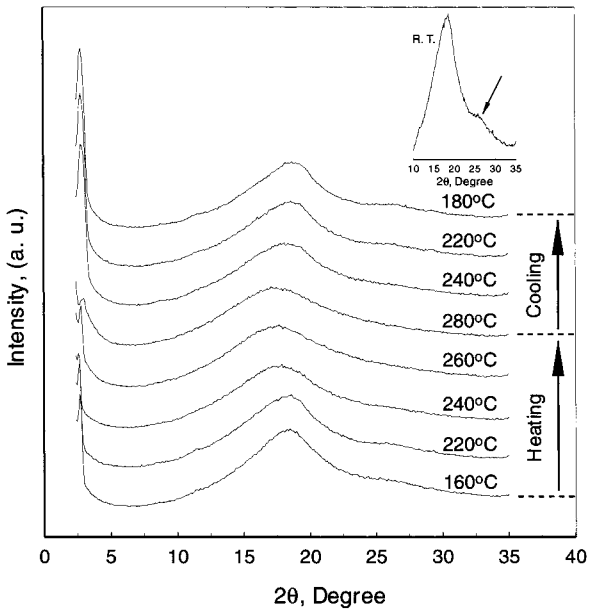

Figure 8. WAXD powder profiles for PAI37 during heating and cooling.

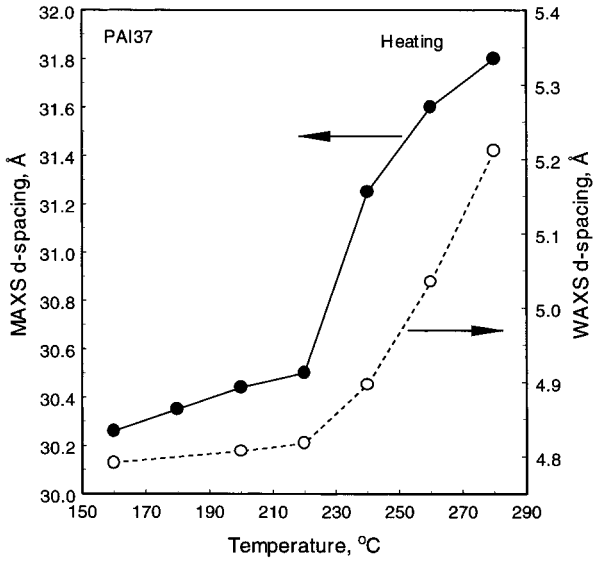

Figure 9. Change of MAXS and WAXS *d* spacings during heating.

~30.2 Å and is typical for the layered smectic structure. The layer *d* spacing in PAI37 is quite similar to that in the liquid crystalline homopolyimide PMDA−BACB.[35] The layer *d* spacing in PMDA−BACB was reported to be 30.87 Å, and the tilting angle was 20°.[35] Our experimental results on PMDA−BACB indicate a layer *d* spacing of 30.4 Å and a tilting angle of 15 °C. The calculated length of the repeating unit of PMDA−BACB varies from 31.05 Å for the all-trans conformation to 29.3 Å for the energy minimized conformation. These calculation and experimental results show that the whole repeating unit functions as a mesogen. The broad wide-angle X-ray scattering (WAXS) with the typical triangle shape (maximum $2\theta \approx 18.6°$) is known to originate from the liquidlike intermolecular scattering and represents a broad distribution of intermolecular distance. In addition, a very weak and diffusive peak can be distinguished at a scattering angle of $2\theta \approx 27°$ (see the inset in Figure 8). In the literature, it has been attributed to lateral correlation.[35] The WAXD profiles show little changes when the temperature is lower than 220 °C in heating. At 240 °C the WAXS becomes less structured. The diffusive peak at $2\theta \approx 27°$ vanishes, and the hole itself becomes broader, indicating the transition into a less ordered phase. The change of *d* spacing of MAXS at $2\theta \approx 2.92°$ and WAXS at $2\theta \approx 18.6°$ during heating is plotted in Figure 9. The *d* spacing from the layered structure slightly increases when the temperature is lower than 220 °C. However, it increases rapidly when the temperature is higher than 220 °C. The fast increase of this MAXS *d* spacing is resulted from the transition from S_C to S_A phase. Assuming that PAI37 has a tilting angle of 15° similar to PMDA−BACB, the MAXS *d* spacing should increase from 30.2 to 31.3 Å when the transition from S_C to S_A completes, if the thermal expansion is not taken into account. The experimental results in Figure 9 indicate an increase from 30.6 to 31.8 Å, agreeable with the calculated results. The intensity of the MAXS decreases considerably when the sample is heated to 280 °C, and this scattering peak vanishes when the temperature is above 285 °C, corresponding to the isotropization process. The MAXS before the sample becomes isotropic melt proves the existence of smectic phases. These WAXD observations together with the results from DSC and PLM experiments have almost excluded the existence of nematic phase before isotropization. The *d* spacing from WAXS shows a larger increase with temperature due to thermal expansion when the temperature is higher than 220 °C. The XRD fiber pattern is shown in Figure 10a. The fiber was pulled from the anisotropic melt at 258 °C without annealing. To our surprise, the scattering spots can be found on both equator and meridian. An integration along both meridian and equator direction can give the intensity maxima at $2\theta = 2.92°$, which is consistent with the MAXS result from the powder sample. The azimuthal scattering intensity along $2\theta = 2.92°$ is stronger on the equator than on the meridian (Figure 10b), which means that the polymer chains are aligned perpendicular to the fiber direction. In a recent XRD report on the drawing of a S_{CA} liquid crystalline polymer,[44] it was found that the MAXS patterns were highly dependent on the strain rates. At a high drawing rate of 50 cm/min, the diffraction spots only appeared on the meridian. When the drawing rate was lowered to 1 cm/min, the diffraction spots were observable on both meridian and equator. Further decreasing the drawing rate to 0.1 cm/min, the diffraction spots were found only on the equator. This anomalous chain orientation was first reported in the oriented polyester that showed a S_{CA} phase[45] and later observed in nematic[46] and S_C[32] liquid crystalline polymers.

Rheology of polymers is the science that studies the deformation and flow of polymer materials in liquid, melt, or solid form, in terms of the polymer materials' elasticity and viscosity. Because of the presence of different ordered structures in the phase transition process in liquid crystalline polymers, the rheological properties are expected to be different to reflect these structural changes. The change of storage (G') and loss (G'') modulus as a function of temperature is shown in Figure 11. The sample was melted and slowly pressed at 320 °C. The cooling process from 320 to 200 °C was performed first and followed by heating. An obvious transition in the heating scan occurs around 274 °C, which corresponds to the isotropization temperature. Careful examination would find two small transitions existing on the G'' curve, which appear around 235 and

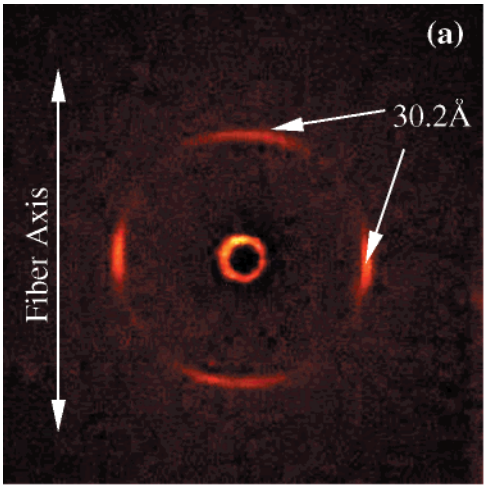

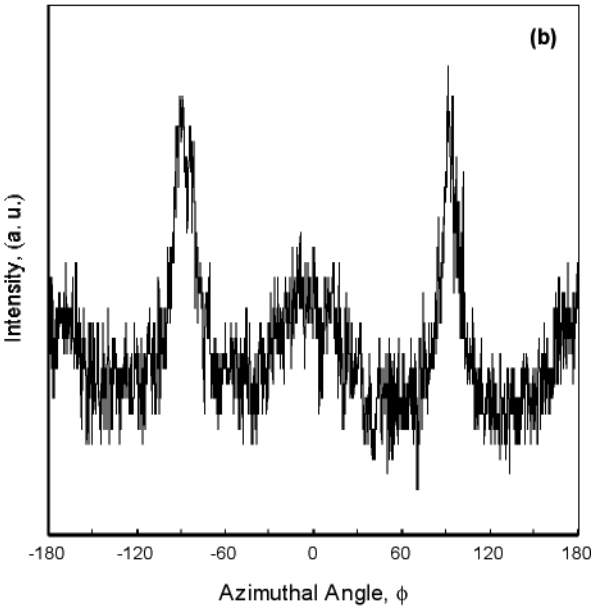

Figure 10. WAXD fiber pattern focusing on the low angle region.

263 °C as the slope changes at these two temperatures. These two small transitions show good agreement with the phase transition temperatures observed in the DSC, PLM, and WAXD experiments (Table 1). The factor that the change in G' at 235 °C is indistinct may be resulted from the low crystallinity in the sample as evidenced by a small enthalpy change ($\Delta H = 1.67$ J/g) in the DSC experiment. On the other hand, during the cooling process, the abrupt increases in G' (or G'') at 257 and 222 °C by more than 1 order of magnitude agree well with the isotropic to mesophase and mesophase to crystalline phase transition observed in the corresponding DSC and WAXD cooling experiments. It is also noticed from the cooling curve that the viscosity does not show a decrease upon the first mesophase formation at 257 °C, which has been observed in the I → N transition in many thermotropic liquid crystalline polymers.[31,47] This observation further excludes the formation of a nematic phase and confirms that the first mesophase formed from the isotropic melt is a smectic phase.

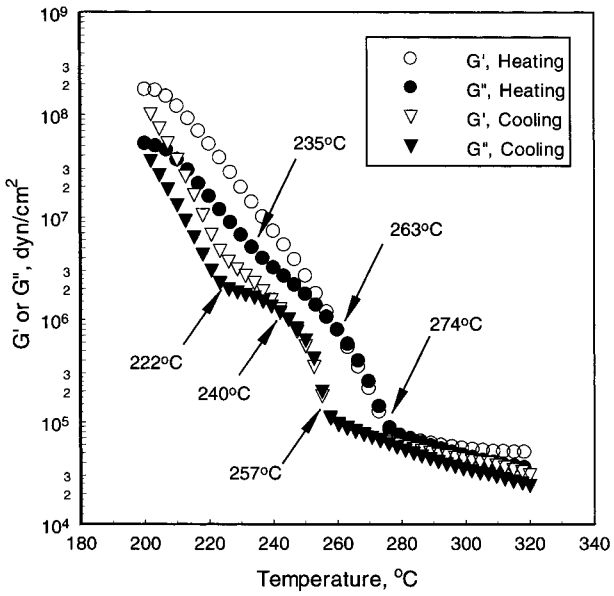

Figure 11. Change of storage (G') and loss (G'') modulus during heating and cooling process.

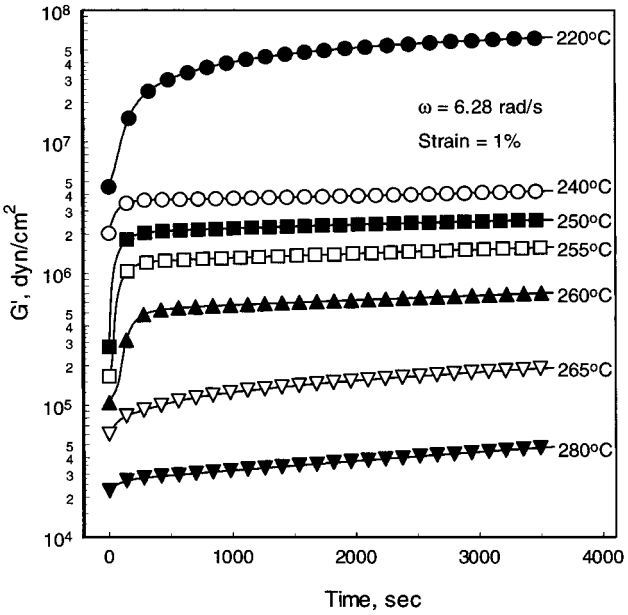

Figure 12. Change of G' during isothermal oscillation at different temperatures.

The change of G' during time sweep at different temperatures is shown in Figure 12. G' increases very little during time sweep when the temperature is at 265 °C or higher. At the temperature range of 260−250 °C, G' increases about 1 order of magnitude initially and then maintains almost constant. The rapid increase in G' in the initial stage at these temperatures should result from the formation of ordered smectic phase. G' shows little dependence on time after the formation of smectic phase. G', in the mesophase temperature range, is about 1−2 orders of magnitude smaller than that for the crystalline phase formation at 220 °C. A gradual increase in G' is also noticed at 220 °C. This should be resulted from the gradual perfection of crystals during annealing, which is reflected as the increase of melting enthalpy in the DSC experiments in Figure 4. The subsequent heating curves after isothermal oscillation at different temperatures for 1 h are plotted in Figure 13. The transitions become prominent after annealing

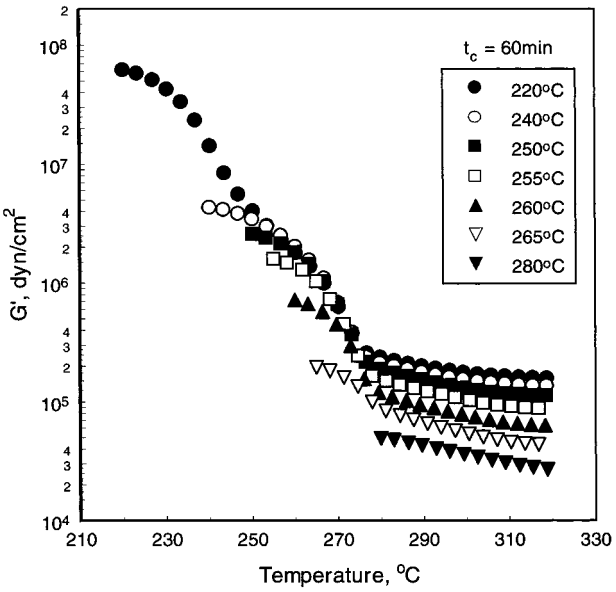

Figure 13. Change of G' during subsequent heating after isothermal oscillation at different temperatures for 60 min.

compared with that shown in Figure 11. The transitions observed from these rheological heating curves are in accordance with the DSC heating curves.

3.2. Transition Kinetics. The transition kinetics for the mesophase and the crystalline phase formation is further investigated by DSC method. The phase transition kinetics for both mesophase formation and three-dimensional crystalline phase formation can be analyzed by the Avrami equation.[48,49]

$$X_{(t)} = 1 - \exp(-kt^n) \tag{1}$$

where $X_{(t)}$ is the crystallized mass fraction in material, k is a temperature-dependent rate constant, t represents time, and n describes the mode of nucleation and crystal growth and is usually an integer between 1 and 4 for different nucleation and crystallization mechanisms. It has also been observed that n is a fraction due to secondary crystallization or crystal perfection. In the isothermal crystallization study by DSC, $X_{(t)}$ is expressed as

$$X_{(t)} = \frac{\Delta H_t}{\Delta H_0} = \frac{\int_0^t E_t \, dt}{\int_0^\infty E_t \, dt} \tag{2}$$

where ΔH_t is the enthalpy change at time t, ΔH_0 is the total enthalpy change of the system, and E_t is the rate of energy evolution at time t.

The exothermic traces can be recorded at selected isothermal temperatures. An integration of these curves can generate the plots of relative crystallinity vs time. From the relative crystallinity vs time plots, the double-logarithm graph for the Avrami exponent determination can be obtained.[37] Shown in Figure 14a are the plots for the mesophase formation at a narrow temperature range from 264 to 267 °C. The Avrami exponent n has an average value of 1.7. PLM observation indicates a random formation of mesophase from the isotropic melt, which means an athermal nucleation. The Avrami exponent ~1.7 suggests a two-dimensional mesophase growth. This result is consistent with the observations from the isotropic melt to smectic phase formation in

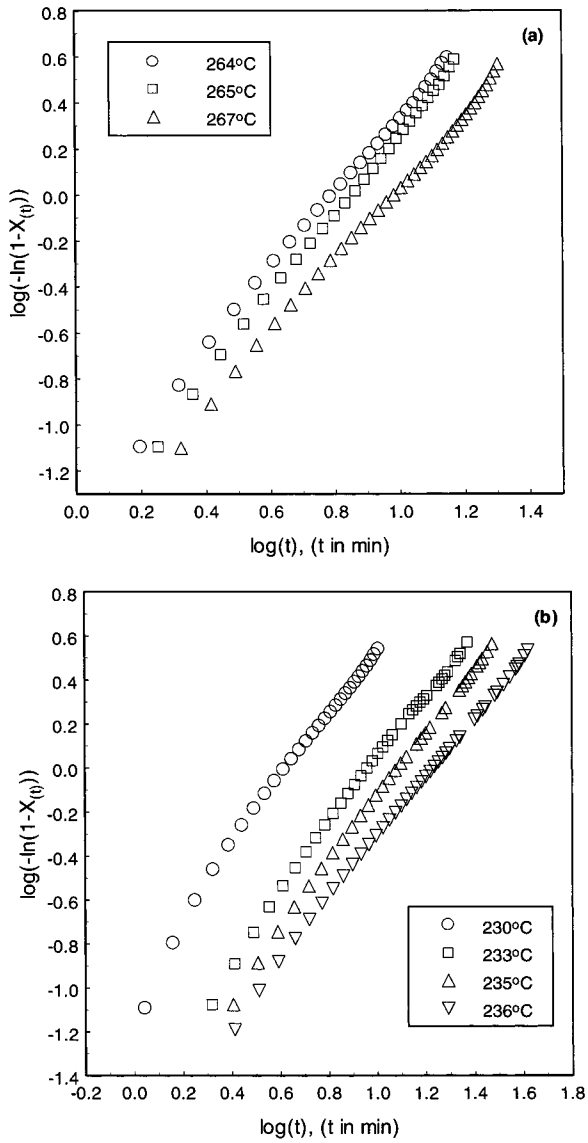

Figure 14. Double-log plots for the determination of the Avrami parameters for the (a) mesophase and (b) crystalline phase formation.

side-chain and main-chain liquid crystalline polymers.[26,50] Figure 14b shows the double-logarithm plots for the crystalline phase formation at the temperature range from 230 to 236 °C. The Avrami component shows an average value of 1.45. At these crystallization temperatures, the mesophase has already formed when the sample was cooled from the isotropic melt. The crystallization process at 230 to 236 °C should start on the ordered smectic phase. Therefore, the dimensionality for the crystallization starting from the mesophase should be smaller than that starting from the isotropic melt. When the mesophase is formed, the system viscosity will increase by more than 1 order of magnitude as shown in Figure 11. The crystallization process is therefore controlled by the chain diffusion.

4. Conclusion

The complicated phase transition behavior of copoly(amide−imide) (PAI37) was investigated by DSC, PLM, XRD, and rheological characterization. PAI37 forms smectic C phase upon melting around 220 °C. The smectic C phase starts to transform into smectic A phase when it is heated to 237 °C. The transformation from

S_C to S_A spans a wide temperature range in which the S_A phase disappears and forms isotropic melt. No nematic phase was observed during heating or cooling process. The WAXD fiber pattern of PAI37 pulled from the anisotropic melt exhibited an anomalous chain orientation, which was characterized by its layer normal perpendicular to the fiber direction. The crystallization behavior for the mesophase and crystalline phase formation was further studied. The Avrami exponent for the mesophase formation was about 1.7, which suggests an athermal nucleation followed by two-dimensional smectic phase growth.

Acknowledgment. The authors thank Ms. Tan G. K. at the Department of Chemistry, National University of Singapore, for her assistance in the XRD experiments. We deeply appreciate the comments and suggestions from the reviewers.

References and Notes

(1) Kricheldorf, H. R. Liquid Crystalline Polyimides. In *Advances in Polymer Science: Progress in Polyimide Chemistry II*; Springer-Verlag: Berlin, 1999; Vol. 141, pp 83−188.
(2) Ghosh, M. K.; Mittal, K. L. *Polyimides: Fundamentals and Applications*; Marcel Dekker: New York, 1996.
(3) Wilson, D.; Stenzenberger, H. D.; Hergenrother, P. M. *Polyimides*; Blackie & Son: 1990.
(4) Evans, J. R.; Orwoll, R. A.; Tang, S. S. *J. Polym. Sci., Polym. Chem. Ed.* **1985**, *23*, 971−980.
(5) Inoue, T.; Kakimoto, M. A.; Imai, Y.; Watanabe, J. *Macromol. Chem. Phys.* **1997**, *198*, 519−530.
(6) Kricheldorf, H. R.; Pakull, R. *Macromolecules* **1988**, *21*, 551−557.
(7) Reinecke, H.; de la Campa, J. G.; de Abajo, J.; et al. *Polymer* **1996**, *37*, 3101−09.
(8) Kricheldorf, H. R.; Gurau, M. *J. Polym. Sci., Part A: Polym. Chem.* **1995**, *33*, 2241−50.
(9) Kricheldorf, H. R.; Probst, N.; Wutz, C. *Macromolecules* **1995**, *28*, 7990−7995
(10) Kricheldorf, H. R.; Pakull, R.; Buchner, S. *J. Polym. Sci., Part A: Polym. Chem.* **1989**, *27*, 431−446.
(11) Kricheldorf, H. R.; Pakull, R. *J. Polym. Sci., Polym. Lett. Ed.* **1985**, *23*, 413−419.
(12) Schwarz, G.; Thomsen, S.; Wutz, C.; Kricheldorf, H. R. *Acta Polym.* **1998**, *49*, 162−173.
(13) Wutz, C.; Gieseler, D.; Maevis, T.; Stribeck, N. *Macromolecules* **1999**, *32*, 4658−4667.
(14) Kricheldorf, H. R.; Probst, N.; Schwarz, G.; Wutz, C. *Macromolecules* **1996**, *29*, 4234−40.
(15) Wutz, C.; Thomsen, S.; Schwarz, G.; Kricheldorf, H. R. *Macromolecules* **1997**, *30*, 6127−33.
(16) Sato, M.; Hirata, T.; Mukaiha, K. I. *Markromol. Chem.* **1992**, *193*, 1729−37.
(17) Asanuma, T.; Oikawa, H.; Ookawa, Y.; Yamaguchi, A. *Polym. Prepr.* **1993**, *34*, 827−828.
(18) Asanuma, T.; Oikawa, H.; Ookawa, Y.; Yamasita, W.; Matsuo, M.; Yamaguchi, A. *J. Polym. Sci., Part A: Polym. Chem.* **1994**, *32*, 2111−18.
(19) Tamai, S.; Ookawa, Y.; Yamaguchi, A. *40th International SAMPE Symposium and Exhibition* **1995**, *40*, 1412−24.
(20) Tamai, S.; Ohkawa, Y.; Yamaguchi, A. *Polymer* **1997**, *38*, 4079−84.
(21) Hudson, S. D.; Lovinger, A. J.; Larson, R. G.; Davis, D. D.; Garay, R. O.; Fujishiro, K. *Macromolecules* **1993**, *26*, 5643−5650.
(22) Yonetake, K.; Sagiya, T.; Koyama, K.; Masuko, T. *Macromolecules* **1992**, *25*, 1009−1010.
(23) Noel, C.; Friedrich, C.; Laupretre, F.; Gillard, J.; Bosio, L.; Strazielle, C. *Polymer* **1984**, *25*, 263−273.
(24) Bhowmik, P. K.; Atkins, E. D. T.; Lenz, R. W. *Macromolecules* **1993**, *26*, 447−451.
(25) Jin, J. I.; Kang, C. S. *Prog. Polym. Sci.* **1997**, *22*, 937−973.
(26) Pardey, R.; Zhang, A. Q.; Gabori, P. A.; Harris, F. W.; Cheng, S. Z. D.; Adduci, J.; Facinelli, J. V.; Lenz, R. W. *Macromolecules* **1992**, *25*, 5060−68.
(27) Pardey, R.; Shen, D. X.; Gabori, P. A.; Harris, F. W.; Cheng, S. Z. D.; Adduci, J.; Facinelli, J. V.; Lenz, R. W. *Macromolecules* **1993**, *26*, 3687−97.
(28) Pardey, R.; Wu, S. S.; Chen, J. H.; Harris, F. W.; Cheng, S. Z. D.; Keller, A.; Adduci, J.; Facinelli, J. V.; Lenz, R. W. *Macromolecules* **1994**, *27*, 5794−02.
(29) Kim, S. O.; Jeoh, B. H.; Chung, I. J. *Polymer* **2001**, *42*, 3249−57.
(30) Kim, S. O.; Kim, T. K.; Chung, I. J. *Polymer* **2000**, *41*, 4709−4717.
(31) Kim, S. O.; Chung, I. J. *Macromolecules* **2000**, *33*, 7549−56.
(32) Leland, M.; Wu. Z. Q.; Chhajer, M.; Ho. R. M.; Cheng, S. Z. D.; Keller, A.; Kricheldorf, H. R. *Macromolecules* **1997**, *30*, 5249−54.
(33) Leland, M.; Wu. Z. Q.; Ho. R. M.; Cheng, S. Z. D.; Kricheldorf, H. R. *Macromolecules* **1998**, *31*, 22−29.
(34) Schwarz, G.; Sun, S. J.; Kricheldorf, H. R. *Macromol. Chem. Phys.* **1997**, *198*, 3123−35.
(35) Tanaka, M.; Konda, M.; Miyamoto, M.; Kimura, Y.; Yamaguchi, A. *High Perform. Polym.* **1998**, *10*, 147−153.
(36) Liu, S. L.; Chung, T. S.; Goh, S. H.; Torii, Y.; Yamaguchi, A.; Ohta, M. *Polym. Eng. Sci.* **1998**, *38*, 1845−1853.
(37) Liu, S. L.; Chung, T. S.; Lu, L.; Torii, Y.; Oikawa, H.; Yamaguchi, A. *J. Polym. Sci., Part B: Polym. Phys.* **1998**, *36*, 1679−1694.
(38) Liu, S. L.; Chung, T. S.; Oikawa, H.; Yamaguchi, A. J. *Polym. Sci., Part B: Polym. Phys.* **2000**, *38*, 3018−3031.
(39) Pramoda, K. P.; Chung, T. S.; Liu, S. L.; Oikawa, H.; Yamaguchi, A. *Polym. Degrad. Stab.* **2000**, *67*, 365−374.
(40) Righetti, M. C.; Laus, M. *Polymer* **2000**, *41*, 8355−62.
(41) Demus, D.; Richter, L. *Textures of Liquid Crystals*; Verlag Chemie: Weinheim, 1978.
(42) Gray, G. W.; Goodby, J. W. G. *Smectic Liquid Crystals: Textures and Structures*; Leonard Hill: Glasgow, 1984.
(43) Kim, G. H.; Pugh, C.; Cheng, S. Z. D. *Macromolecules* **2000**, *33*, 8983−91.
(44) Bello, P.; Bello, A.; Lorenzo, V. *Polymer* **2001**, *42*, 4449−52.
(45) Watanabe, J.; Hayashi, M. *Macromolecules* **1988**, *21*, 278−80.
(46) Romo-Uribe, A.; Windle, A. H. *Macromolecules* **1996**, *29*, 6246−55.
(47) Kim, D. O.; Han, C. D. *Macromolecules* **2000**, *33*, 3349−58.
(48) Avrami, M. *J. Chem. Phys.* **1939**, *7*, 1103.
(49) Avrami, M. *J. Chem. Phys.* **1940**, *8*, 212.
(50) Jonsson, H.; Wallgren, E.; Hult, A.; Gedde, U. W. *Macromolecules* **1990**, *23*, 1041−47.

MA010895F